Acta Crystallographica Section F
Structural Biology and Crystallization Communications
ISSN 1744-3091

Crystallization and initial X-ray diffraction studies of the flavoenzyme NAD(P)H:(acceptor) oxidoreductase (FerB) from the soil bacterium *Paracoccus denitrificans*

Tomáš Klumpler,[a] Vojtěch Sedláček,[b] Jaromír Marek,[a]* Michaela Wimmerová[b] and Igor Kučera[b]

[a]Laboratory of Molecular Plant Physiology, Department of Functional Genomics and Proteomics, Institute of Experimental Biology, Faculty of Science, Masaryk University, Kamenice 5/A2, CZ 625 00 Brno, Czech Republic, and [b]Department of Biochemistry, Faculty of Science, Masaryk University, Kamenice 5/A5, CZ 625 00 Brno, Czech Republic

Correspondence e-mail: marek@chemi.muni.cz

Received 15 December 2009
Accepted 8 February 2010

The flavin-dependent enzyme FerB from *Paracoccus denitrificans* reduces a broad range of compounds, including ferric complexes, chromate and most notably quinones, at the expense of the reduced nicotinamide adenine dinucleotide cofactors NADH or NADPH. Recombinant unmodified and SeMet-substituted FerB were crystallized under similar conditions by the hanging-drop vapour-diffusion method with microseeding using PEG 4000 as the precipitant. FerB crystallized in several different crystal forms, some of which diffracted to approximately 1.8 Å resolution. The crystals of native FerB belonged to space group $P2_1$, with unit-cell parameters a = 61.6, b = 110.1, c = 65.2 Å, β = 118.2° and four protein molecules in the asymmetric unit, whilst the SeMet-substituted form crystallized in space group $P2_12_12$, with unit-cell parameters a = 61.2, b = 89.2, c = 71.5 Å and two protein molecules in the asymmetric unit. Structure determination by the three-wavelength MAD/MRSAD method is now in progress.

1. Introduction

Enzymes that utilize flavin cofactors [flavin mononucleotide (FMN) or flavin adenine dinucleotide (FAD)] are unique in their ability to catalyze a wide variety of mechanistically different reactions such as dehydrogenation, oxygen activation, halogenation, nonredox conversions, light sensing and emission and DNA repair (Mattevi, 2006). *Paracoccus denitrificans*, a common soil bacterium (Baker *et al.*, 1998), possesses two flavin-dependent enzymes, FerA and FerB, that have ferric reductase activity and are capable of transferring electrons from the reduced form of nicotinamide adenine dinucleotide (NADH) to various ferric iron complexes (Mazoch *et al.*, 2004). Following its identification in the *P. denitrificans* genome (Sedláček *et al.*, 2009*a*), the gene encoding FerB was cloned and successfully expressed in *Escherichia coli* in the form of a C-terminally hexahistidine-tagged fusion protein. Both native and recombinant FerB exhibit comparable molecular activities with ferric nitrilotriacetate as a nonphysiological electron acceptor and exist in solution as stable dimers of two identical subunits, each of which contains one molecule of FAD (Mazoch *et al.*, 2004; Tesařík *et al.*, 2009).

In addition to its activity towards iron(III) compounds, FerB has considerable activity towards benzoquinones and naphthoquinones (Mazoch *et al.*, 2004; Sedláček *et al.*, 2009*b*). Consistent with this observation, an *in silico* search (Sedláček *et al.*, 2009*b*) revealed substantial degrees of homology between the primary structure of FerB and those of several other microbial and plant quinone reductases, all of which are FMN-containing flavoproteins: the chromate reductase ChrR from *Pseudomonas putida* (Park *et al.*, 2000), ChrR (formerly YieF) from *Escherichia coli* (Ackerley *et al.*, 2004), the NADPH:quinone reductase NQR from *Arabidopsis thaliana* (Sparla *et al.*, 1999) and the low-temperature responsive reductase Lot6p from *Saccharomyces cerevisiae* (Sollner *et al.*, 2007). The function of these enzymes in cell metabolism has not yet been fully elucidated. They may catalyze the two-electron reduction of quinones to hydroquinones without the formation of autooxidizable semiquinone radical intermediates and hence, by analogy with the well characterized mammalian NAD(P)H:quinone oxidoreductase (NQO1;

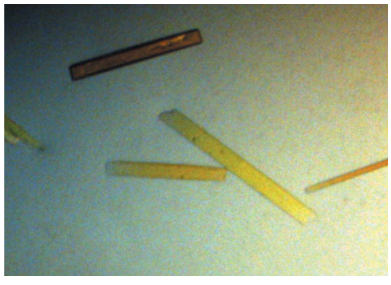

Ross *et al.*, 2000), have been implicated in protecting organisms against redox stress (Sparla *et al.*, 1999; Gonzalez *et al.*, 2005; Sollner *et al.*, 2007). Eukaryotic quinone reductases, including Lot6p, also bind to the core particle of the proteasome and serve as redox switches for controlling the proteosomal degradation of several transcription factors (Sollner & Macheroux, 2009).

Although FerB resembles the four homologous enzymes mentioned above in many respects, there also are noticeable differences: (i) the reduction of naphthoquinones by FerB proceeds *via* a one-electron process, as evidenced by a high level of a flavin semiquinone form of the enzyme, the parallel conversion of O_2 to H_2O_2 and the positive results of a test using cytochrome *c* as a superoxide trap (Sedláček *et al.*, 2009*b*), (ii) the catalytic cofactor of FerB is FAD (Mazoch *et al.*, 2004) and not FMN and (iii) an amino-terminally tagged FerB polypeptide neither binds flavin nor dimerizes (Tesařík *et al.*, 2009), which suggests that in the case of FerB the free N-terminus is required for assembly of the enzyme to occur.

Determining the molecular basis for these differences and obtaining further details of catalysis by FerB would be greatly aided by knowledge of the three-dimensional structure of the enzyme. The present work presents the crystallization and preliminary X-ray analysis of FerB as a first step towards this goal.

2. Materials and methods

2.1. Production of native and selenomethionine-substituted FerB in *E. coli*

C-terminally His_6-tagged FerB was produced in *E. coli* BL21 (DE3) pLysS host cells transformed with the *ferB* expression vector pET21a(+)-ferB essentially as described by Tesařík *et al.* (2009). In parallel with the native form, selenomethionine-substituted FerB was prepared using the methionine-biosynthesis inhibition method (Van Duyne *et al.*, 1993). A 10 ml aliquot of a culture grown overnight at 310 K in LB medium was centrifuged (1 min, 5000*g*); the pellet was resuspended in 1 ml M9 minimal medium and added to 1 l of the same medium containing glucose [0.4%(*w*/*v*)] and ampicillin (100 mg l^{-1}). The culture was shaken in a 3 l flask at 310 K until it reached an OD_{600} of 0.6, at which point selenomethionine (50 mg), lysine hydrochloride (100 mg), leucine (50 mg), isoleucine (50 mg), threonine (100 mg), valine (50 mg) and isopropyl β-D-1-thiogalactopyranoside (1 m*M* final concentration) were added. After an additional 20 h of growth, the cells were harvested by centrifugation (6 min, 9000*g*) and washed with buffer *A* containing 10 m*M* imidazole, 50 m*M* sodium phosphate, 300 m*M* NaCl pH 8.0 supplemented with 2 m*M* dithiothreitol in the case of SeMet-FerB. Frozen resuspended cells were disrupted with an X-press (AB Biox). The soluble fraction containing His-tagged FerB was separated from insoluble material by centrifugation (40 min, 120 000*g*).

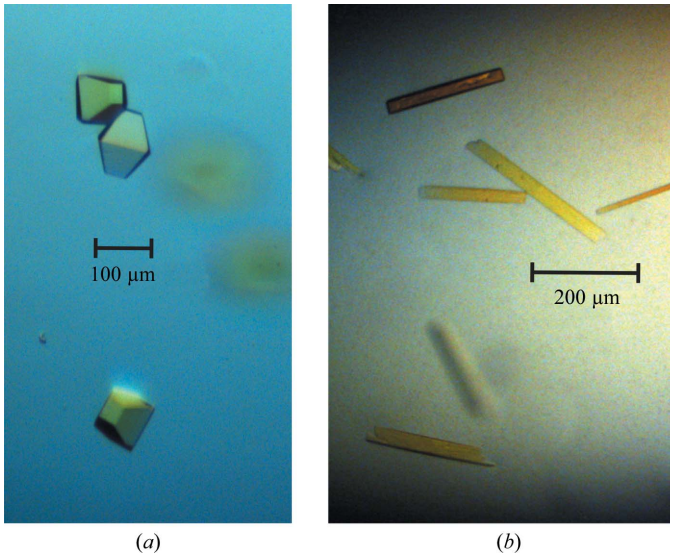

(*a*) (*b*)

Figure 1
Typical crystals of FerB. (*a*) Poorly diffracting octahedral form, (*b*) rod-like form used for data collection.

2.2. Protein purification

Both native and selenomethionine-substituted FerB were purified in a single chromatography step using a HisPrep FF 16/10 column (GE Healthcare; Tesařík *et al.*, 2009). Elution under standard conditions (0.5 *M* imidazole in buffer *A* supplemented with 2 m*M* dithiothreitol in the case of SeMet-FerB) resulted in almost homogenous protein preparations (>95% homogeneity). The effectiveness of purification was monitored by SDS–PAGE and the purity of the final preparations was estimated by densitometry of the Coomassie Brillant Blue-stained gels. The protein concentration was determined according to Lowry *et al.* (1951) with bovine serum albumin as a standard.

2.3. MALDI–TOF mass spectrometry

Native and selenomethionine-substituted FerB were analyzed by matrix-assisted laser desorption/ionization time-of-flight (MALDI–TOF) mass spectrometry on a Ultraflex III mass spectrometer (Bruker Daltonics, Germany). Samples were cocrystallized with 2,5-dihydroxybenzoic acid and analyzed in linear mode using an accelerating voltage of 25 kV. The instrument was calibrated with $[MH]^+$ and $[MH]^{2+}$ peaks using a mixture of peptide standards (Bruker Daltonics). The peaks at molecular masses of 21 289 and 21 616 detected for native and selenomethionine-substituted FerB corresponded well to the predicted mass difference of 328 Da (seven methionine residues per chain).

2.4. Crystallization

Preliminary screening of crystallization conditions for native FerB was carried out in sitting drops (100 nl protein solution mixed with 100 nl reservoir solution equilibrated against 100 µl reservoir solution) at 293 K in 96-well Innovaplate SD-2 plates using an automated nanolitre liquid-handling system (Mosquito, TTP LabTech) and several commercially available screening sets (Structure Screen I and II HT-96, MemStart and MemSys HT-96 and PACT premier HT-96 from Molecular Dimensions and JBScreen Classic HTS I and II from Jena Biosciences GmbH); approximately 500 individual conditions were tested. Promising microcrystals were obtained after a few days from condition E3 [0.1 *M* sodium acetate, 0.2 *M* ammonium sulfate, 22%(*w*/*v*) PEG 4000] of JBScreen Classic HTS I (Jena Biosciences GmbH).

Optimization of the initial conditions was required to increase the size of the crystals and to improve the crystal quality. We employed a microseeding technique for crystallization of the FerB protein. At the start of the procedure, two bunches of microcrystals of native FerB were transferred into 200 µl stabilizing solution [14%(*w*/*v*) PEG 4000, 0.2 *M* ammonium sulfate, 0.1 *M* sodium acetate, 0.1 *M* MES buffer pH 5.00] and crushed with a seed bead (Seed Bead Kit, Hampton Research). The same stabilizing solution was used for cross-microseeding of SeMet-FerB with starting seeds prepared by crushing two

crystals of native protein. In all of the subsequent optimization steps we prepared seeds from two good-looking 'fresh' crystals obtained in the previous optimization run. Two forms of FerB crystals were grown in EasyXtal 24-well plates (Qiagen) by the hanging-drop vapour-diffusion method, in which drops containing a 1:1:1 (by volume) mixture of protein solution, reservoir solution and seed stock-containing solution were equilibrated against 1 ml reservoir solution at 293 K.

The optimized conditions obtained as a result of approximately 300 individual crystallization experiments were the same for both the native and SeMet protein and consisted of PEG 4000 in the concentration range 13–16%(*w*/*v*), 0.2 *M* ammonium sulfate, 0.1 *M* sodium acetate and 0.1 *M* MES buffer pH 5.0. Using these conditions, crystals with representative dimensions of 0.1 × 0.1 × 0.1 mm and 0.2–0.3 × 0.05 × 0.03 mm and several different crystal morphologies (see Fig. 1) were grown in 3–4 d.

2.5. Data collection and processing

We used beamline X13 of the DORIS-III storage ring at EMBL/DESY (Hamburg, Germany) operating at a fixed wavelength of 0.8123 Å for the collection of the first data set from native FerB, while a MAD data set was collected from a single crystal of SeMet-FerB on the tuneable beamline X12 of the same storage ring. Prior to data collection, a measured crystal was transferred directly from the mother liquor into a cold nitrogen stream (100 K). Both data sets were collected using CCD detectors (MAR SX-165 on X13 and MAR MX-225 on X12; MAR Research) in dose mode with an oscillation angle of 0.5°. The crystal-to-detector distance was 160 mm for FerB and 180 mm for SeMet-FerB. A total of 300 images were collected for native FerB. Using the seleniomethionine-derivative crystals, we collected 2 × 400 images at the peak of the selenium absorption edge and at the inflection point, but gradually increasing radiation damage to the SeMet-FerB crystal only allowed us to collect 300 frames at a wavelength on the high-energy side of the absorption edge. All data were processed and merged using the *XDS* system (Kabsch, 1993) with the instruction FRIEDEL'S_LAW=FALSE. The data-collection statistics are summarized in Table 1. Before beginning the search for heavy-atom sites, data were scaled with *SCALEIT* (Howell & Smith, 1992) as implemented in the *CCP*4 program suite (Collaborative Computational Project, Number 4, 1994).

3. Results and discussion

Several crystal forms of FerB with different diffraction qualities were obtained (Fig. 1). While an octahedral/cubic form of FerB with representative crystal dimensions of 0.1 × 0.1 × 0.1 mm (Fig. 1*a*) diffracted poorly or did not diffract at all, rod-like crystals of FerB or SeMetFerB with typical dimensions of 0.2–0.3 × 0.05 × 0.03 mm (Fig. 1*b*) diffracted very well, typically to a resolution significantly below 2 Å (see Fig. 2*a* and statistics in Table 1). We also applied cryoprotectants (*e.g.* PEG 400, glycerol or Paratone-N), but the resolution of the data collected during experiments with cryoprotectant was considerably poorer (typically below 3 Å) than that from crystals without cryoprotectant.

The rod-like crystal of native FerB used for data collection belonged to the monoclinic space group $P2_1$. The asymmetric unit was estimated to contain four (V_M = 2.29 Å^3 Da^{-1}) molecules (Matthews, 1968); the estimated solvent content was approximately 46.2%. We tried to solve the FerB structure by molecular-replacement (MR) methods using an NAD(P)H-dependent FMN reductase flavoprotein from *P. aeruginosa* PA01 (PDB code 1rtt; Agarwal *et al.*, 2006) identified by a *FASTA* search (Pearson & Lipman, 1988) as a model. Unfortunately, all MR trials were unsuccessful. We therefore collected data from a selenomethionine derivative of FerB. The crystal of SeMet-FerB used for MAD data collection belonged to the orthorhombic space group $P2_12_12$. The asymmetric unit was estimated to contain two (V_M = 2.29 Å^3 Da^{-1}) molecules, with an estimated solvent content of approximately 46.3%. The wavelengths used for MAD data collection were chosen from X-ray fluorescence spectra and the slow radiation decay of the Se-Met FerB crystal at 100 K allowed us to collect three data sets: at the peak of the Se absorption edge, at the inflection point of the edge and away from the

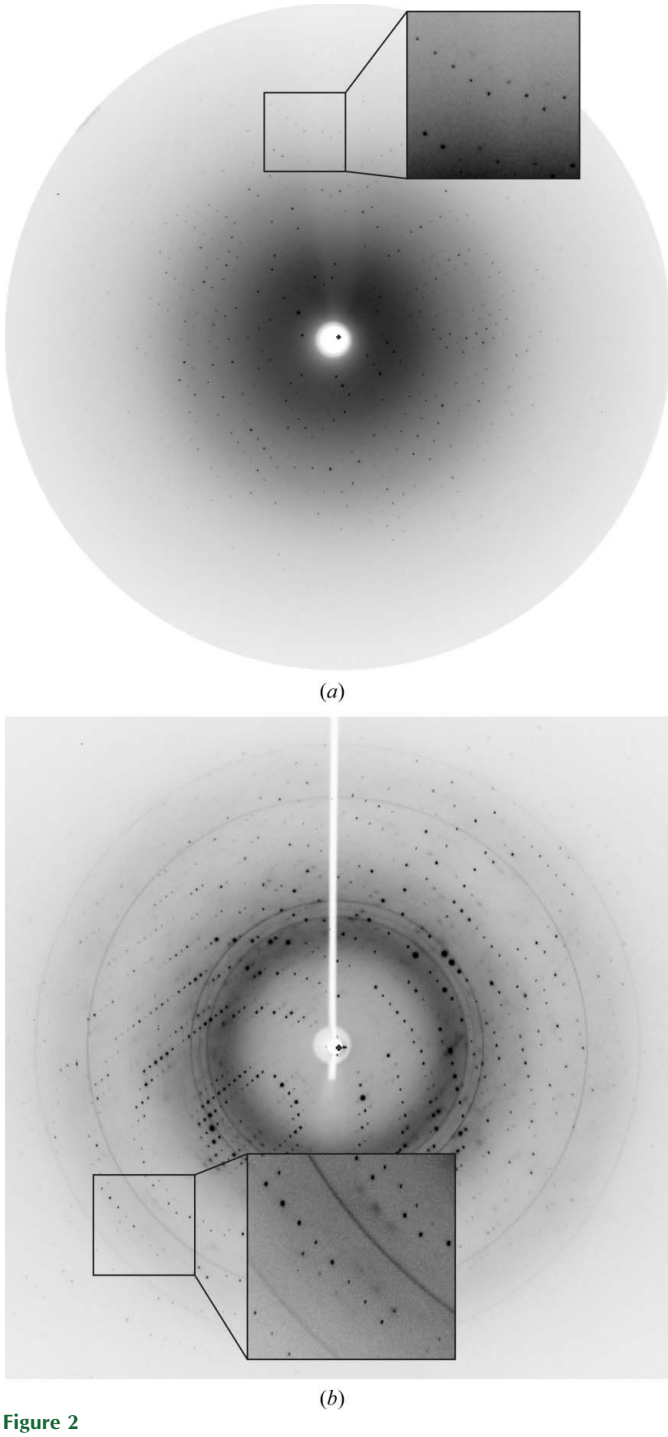

Figure 2
Typical diffraction images for FerB. (*a*) Native form. (*b*) SeMet-substituted FerB.

Table 1
Data-collection statistics.

Values in parentheses are for the highest resolution shell. Observed reflections are those for which $I > 2\sigma(I)$. The resolution ranges 3.69–3.65, 3.46–3.42, 2.69–2.65, 2.27–2.23 and 1.963–1.863 were excluded for the de-iced MAD data.

		MAD data		
	Native data	Peak	Inflection point	High-energy remote
Wavelength (Å)	0.8123	0.97714	0.977530	0.97522
Resolution (Å)	19.6–1.77 (1.80–1.77)	30–1.75 (1.75–1.78)	30–1.75 (1.75–1.78)	30–1.75 (1.75–1.78)
Space group	$P2_1$	$P2_12_12$		
Unit-cell parameters				
a (Å)	61.62	61.22		
b (Å)	110.11	89.19		
c (Å)	65.15	71.46		
β (°)	118.23	90		
Molecules in asymmetric unit	4	2		
Measured reflections	235649 (8894)	240954 (4683)	240741 (4715)	128903 (2518)
Unique reflections	73485 (3304)	65637 (2476)	65504 (2489)	61449 (1970)
Unique observed reflections	65896 (1993)	47601 (1065)	50366 (859)	44063 (551)
Completeness (all/observed)	98.4/88.3 (89.5/69.9)	86.1/68.0 (65.5/26.7)	85.8/66.0 (65.8/22.7)	80.5/57.7 (52.2/14.6)
Mean $I/\sigma(I)$ (all/observed)	17.8/19.7 (3.2/4.8)	14.8/18.6 (2.2/4.3)	14.0/18.0 (1.8/4.0)	10.7/14.8 (1.4/3.5)
Redundancy	3.2	3.7	3.7	2.1
$R_{\rm merge}$† (all/observed) (%)	4.8/4.6 (35.6/25.9)	5.7/5.1 (33.7/19.2)	6.0/5.3 (41.2/21.1)	5.2/4.3 (41.7/19.5)
De-iced MAD data				
Measured reflections		221676 (4666)	222186 (4703)	119137 (2514)
Unique reflections		58529 (2468)	58746 (2486)	55412 (1965)
Unique observed reflections		47601 (1065)	46637 (930)	41223 (581)
Completeness (all/observed)		76.8/62.4 (62.3/28.2)	77.0/61.1 (65.6/24.5)	72.6/54.0 (52.1/15.4)
Mean $I/\sigma(I)$ (all/observed)		16.7/20.4 (2.3/4.5)	16.1/20.1 (1.9/4.1)	12.6/16.7 (1.5/3.7)
Redundancy		3.8	3.8	2.2
$R_{\rm merge}$† (all/observed) (%)		5.4/4.9 (32.4/18.8)	5.7/5.0 (39.4/21.1)	4.8/4.1 (39.7/19.6)

† $R_{\rm merge} = \sum_{hkl}\sum_i |I_i(hkl) - \langle I(hkl)\rangle| / \sum_{hkl}\sum_i I_i(hkl)$, where $I_i(hkl)$ is the intensity of reflection hkl and $\sum_i$ is the sum over all i measurements of reflection hkl.

edge at a wavelength on the high-energy side of the edge. As seen in Fig. 2(*b*) and Table 1, the SeMet-FerB diffraction data collected to 1.75–1.80 Å resolution have only one potential weak point: the weak ice rings at resolutions of 3.69–3.65, 3.46–3.42, 2.69–2.65, 2.27–2.23 and 1.963–1.863 Å. Structure determination of FerB is now in progress using the three-wavelength MAD and MRSAD methods as implemented in *Auto-Rickshaw*, the EMBL-Hamburg automated crystal structure-determination platform (Panjikar *et al.*, 2005, 2009).

We wish thank EMBL/DESY Hamburg for providing us with synchrotron facilities and D. Tucker for his assistance with data collection on beamlines X12 and X13 of the DORIS-III storage ring at DESY Hamburg. The authors are grateful to Ondrej Šedo for measuring the MALDI–TOF MS spectra and the Meta Center (http://meta.cesnet.cz) for computer time. This research was supported by grants from the Czech Science Foundation (grant Nos. 204/08/H054 and 525/07/1069) and the Ministry of Education, Youth and Sports (grant Nos. MSM0021622413 and MSM0021622415).

References

Ackerley, D. F., Gonzalez, C. F., Park, C. H., Blake, R. II, Keyhan, M. & Matin, A. (2004). *Appl. Environ. Microbiol.* **70**, 873–882.
Agarwal, R., Bonanno, J. B., Burley, S. K. & Swaminathan, S. (2006). *Acta Cryst.* D**62**, 383–391.
Baker, S. C., Ferguson, S. J., Ludwig, B., Page, M. D., Richter, O. M. & van Spanning, R. J. (1998). *Microbiol. Mol. Biol. Rev.* **62**, 1046–1078.
Collaborative Computational Project, Number 4 (1994). *Acta Cryst.* D**50**, 760–763.
Gonzalez, C. F., Ackerley, D. F., Lynch, S. V. & Matin, A. (2005). *J. Biol. Chem.* **280**, 22590–22595.
Howell, P. L. & Smith, G. D. (1992). *J. Appl. Cryst.* **25**, 81–86.
Kabsch, W. (1993). *J. Appl. Cryst.* **26**, 795–800.
Lowry, O. H., Rosebrough, N. J., Farr, A. L. & Randall, R. J. (1951). *J. Biol. Chem.* **193**, 265–275.
Mattevi, A. (2006). *Trends Biochem. Sci.* **31**, 276–283.
Matthews, B. W. (1968). *J. Mol. Biol.* **33**, 491–497.
Mazoch, J., Tesařík, R., Sedláček, V., Kučera, I. & Turánek, J. (2004). *Eur. J. Biochem.* **271**, 553–562.
Panjikar, S., Parthasarathy, V., Lamzin, V. S., Weiss, M. S. & Tucker, P. A. (2005). *Acta Cryst.* D**61**, 449–457.
Panjikar, S., Parthasarathy, V., Lamzin, V. S., Weiss, M. S. & Tucker, P. A. (2009). *Acta Cryst.* D**65**, 1089–1097.
Park, C. H., Keyhan, M., Wielinga, B., Fendorf, S. & Matin, A. (2000). *Appl. Environ. Microbiol.* **66**, 1788–1795.
Pearson, W. R. & Lipman, D. J. (1988). *Proc. Natl Acad. Sci. USA*, **85**, 2444–2448.
Ross, D., Kepa, J. K., Winski, S. L., Beall, H. D., Anwar, A. & Siegel, D. (2000). *Chem. Biol. Interact.* **129**, 77–97.
Sedláček, V., van Spanning, R. J. M. & Kučera, I. (2009*a*). *Microbiology*, **155**, 1294–1301.
Sedláček, V., van Spanning, R. J. M. & Kučera, I. (2009*b*). *Arch. Biochem. Biophys.* **483**, 29–36.
Sollner, S. & Macheroux, P. (2009). *FEBS J.* **276**, 4313–4324.
Sollner, S., Neubauer, R., Ehammer, H., Prem, A., Deller, S., Palfey, B. A., Daum, G. & Macheroux, P. (2007). *FEBS J.* **274**, 1328–1339.
Sparla, F., Tedeschi, G., Pupilo, P. & Trost, P. (1999). *FEBS Lett.* **463**, 382–386.
Tesařík, R., Sedláček, V., Plocková, J., Wimmerová, M., Turánek, J. & Kučera, I. (2009). *Protein Expr. Purif.* **68**, 233–238.
Van Duyne, G. D., Standaert, R., Karplus, P. A., Schreiber, S. L. & Clardy, J. (1993). *J. Mol. Biol.* **229**, 105–124.